RSC Advances

COMMUNICATION

# Crystal structure, stability and Ago2 affinity of phosphorodithioate-modified RNAs†

Pradeep S. Pallan,[a] Xianbin Yang,*[b] Malgorzata Sierant,[c] N. Dinuka Abeydeera,[b] Tom Hassell,[d] Carlos Martinez,[d] Magdalena Janicka,[c] Barbara Nawrot[c] and Martin Egli*[a]

Cite this: *RSC Adv.*, 2014, **4**, 64901

Received 22nd September 2014
Accepted 18th November 2014

DOI: 10.1039/c4ra10986d

www.rsc.org/advances

Small interfering RNAs (siRNAs) with phosphorodithioate modifications (PS2-RNA) possess favourable properties for use as RNAi therapeutics. Beneficial here is the combining of PS2 and 2′-*O*-methyl modifications (MePS2). SiRNAs with MePS2 moieties in the sense strand show promising efficacies *in vitro* and *in vivo*. Crystal structures of PS2- and MePS2- modified RNAs reveal subtle changes in geometry and hydration compared with natural RNA. A model of an MePS2-RNA–PAZ domain complex points to a hydrophobic effect as the source of the higher affinity of MePS2-RNA for Ago2.

Small interfering RNAs (siRNAs) designed against a wide range of targets, of various formulations, and in many cases comprising chemical modifications are now being evaluated in the clinic.[1–4] Chemical modification of the antisense (guide) and/or sense (passenger) siRNA strand modulates RNA affinity, nuclease resistance, immune stimulation, uptake and biodistribution, and is widely expected to be required for efficacy *in vivo*.[5–9] SiRNAs containing phosphorodithioate modifications (PS2-RNA; Fig. 1) were recently shown to exhibit favorable properties for therapeutic applications.[10] Thus, the PS2 moiety, despite destabilizing the duplex slightly relative to the native phosphate (PO2), appears not to distort the A-form geometry, improves serum stability, and is tolerated in the central part of the antisense strand as well as in most of the positions tested in the sense strand.

Unlike the phosphorothioate moiety (PS; Fig. 1), PS2 is achiral, thus precluding potential drawbacks that may arise from chiral *P*-substituted oligonucleotides, owing to variable biophysical and biochemical properties of individual (*e.g.* PS-) diastereoisomers.[11,12] In addition, PS2-modified siRNAs display increased protection against degradation by nucleases compared with PS-modified oligonucleotides.[10,13,14] Combining the PS2 with the 2′-*O*-methyl ribose modification (MePS2-RNA; Fig. 1) afforded increased loading of modified siRNA duplexes into the RNA-induced silencing complex (RISC) as well as enhanced anti-tumor activity.[15] Interestingly, the former property can be attributed to MePS2 modification at two residues adjacent to the 3′-TT overhang in the sense siRNA strand (ESI Fig. S1†). This conclusion is supported by higher association (based on *in vitro* pull-down assays), and tighter intracellular binding between MePS2-siRNA and Ago2 protein, relative to the corresponding PO2, PS2-, or methoxy-modified RNAs (RNA, PS2-RNA, or Me-RNA, resp.; Fig. 1). MePS2-siRNA showed significantly enhanced silencing of EphA2 involved in taxane resistance compared to all other RNA chemistries (Fig. 1) in both the SKOV3ipl and HeyA8 epithelial ovarian cancer cell lines that highly express target protein.[15] Other proteins with a key role in chemo-resistance besides EphA2, such as GRAMD1B, were subsequently targeted by systemic administration of MePS2-siRNA, leading to a re-sensitization of chemo-resistant ovarian tumors to taxane therapy.[15]

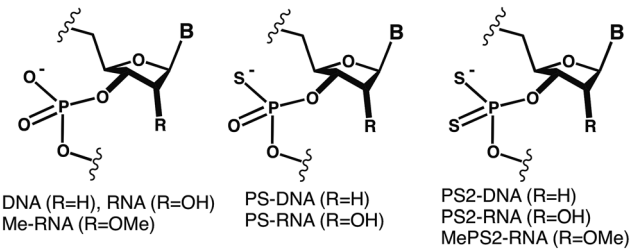


Fig. 1 Structures of native and modified DNA and RNA.

[a]*Department of Biochemistry, Vanderbilt University, School of Medicine, Nashville, TN 37232, USA. E-mail: martin.egli@vanderbilt.edu; Fax: +1-615-322-7122; Tel: +1-615-343-8070*

[b]*AM Biotechnologies LLC, 12521 Gulf Freeway, Houston, TX 77034, USA. E-mail: xianbin.yang@thioaptamer.com; Fax: +1-832-476-0294; Tel: +1-832-379-2175*

[c]*Department of Bioorganic Chemistry, Centre of Molecular and Macromolecular Studies, Polish Academy of Sciences, Lodz, Poland*

[d]*Sigma Life Science, 9186 Six Pines, The Woodlands, Texas 77380, USA*

† Electronic supplementary information (ESI) available: General methods, including crystallographic experiments (Table S1) and model building, and illustrations of EphA2 siRNA (Fig. S1), superimposition of PS2-RNA and RNA duplexes (Fig. S2), CD spectra (Fig. S3), and comparisons between crystal structures of Ago2–siRNA and PAZ–siRNA complexes (Fig. S4). See DOI: 10.1039/c4ra10986d

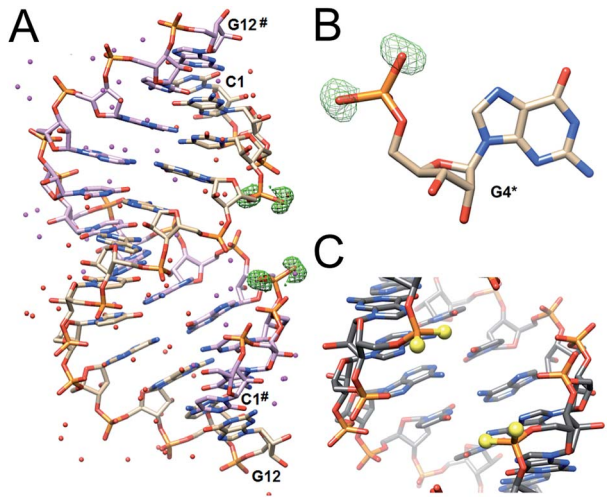


Fig. 2 Crystal structure of the $C_{PS2}$G-RNA duplex. (A) View across the major and minor grooves. Fourier Fo-Fc difference electron density (2.5$\sigma$ level) around O1P and O2P of G4 and G16 (indicating the presence of sulfur) is depicted as a green meshwork, terminal residues are labeled, and water molecules are red spheres. (B) Close-up view of residue G4 with difference density around O1P and O2P before incorporation of sulfur. (C) View into the central major groove with sulfur atoms colored in yellow.

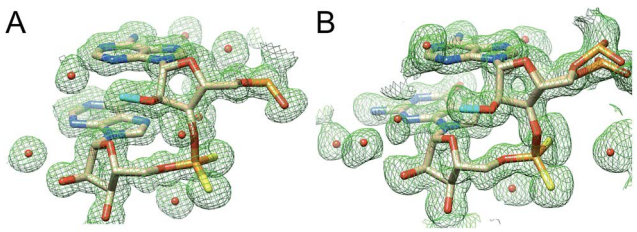


Fig. 3 Close-up views of the MePS2-modified backbones in the (A) $A_{MePS2}$A- and (B) $A_{MePS2}$G duplexes. Fourier (2Fo-Fc) electron density (1.2$\sigma$ level) is depicted as a green meshwork, and 2′-*O*-methyl carbon and sulfur atoms are highlighted in cyan and yellow, respectively.

Table 1 Melting temperatures $T_m$ of native and MePS2-siRNAs

| RNA | Sequence | $T_m$ [°C] |
|---|---|---|
| siRNA-1 | 5′ AUA CAG GCA GCA GUA ACU UU TT 3′<br>3′ TT UAU GUC CGU CGU CAU UGA AA 5′ | 73.7 ± 0.8 |
| MePS2-1 | 5′ AUA CAG GCA GCA GUA ACU<br>$\mathbf{U_{MePS2}U_{MePS2}}$TT 3′<br>3′ TT UAU GUC CGU CGU CAU<br>UGA A A 5′ | 74.0 ± 0.2 |
| MePS2-3 | 5′ AUA C$\mathbf{A_{MePS2}}$GGCAG$\mathbf{_{MePS2}}$CAGUA$\mathbf{_{MePS2}}$ACU<br>UU$\mathbf{_{MePS2}}$TT 3′<br>3′ TT UAU GU C CGUC GUCAU UGA AA 5′ | 73.7 ± 0.5 |
| MePS2-4 | 5′ AUA CAG GCA GCA GUA AC U UU TT 3′<br>3′ TT UAU GUC CGU CGU CAU<br>UG$\mathbf{_{MePS2}A_{MePS2}}$AA 5′ | 74.2 ± 0.8 |
| MePS2-9 | 5′ AUA$\mathbf{_{MePS2}}$CAG GCA GC$\mathbf{A_{MePS2}}$GUA ACU<br>UU TT 3′<br>3′ TT UAU GUC CGU CGU$\mathbf{_{MePS2}}$CAU UGA AA 5′ | 74.4 ± 0.5 |
| MePS2-11 | 5′ AUA C$\mathbf{A_{MePS2}}$GGCAG$\mathbf{_{MePS2}}$CAGUA$\mathbf{_{MePS2}}$ACU<br>UU$\mathbf{_{MePS2}}$TT 3′<br>3′ TT UAU GU CCGU$\mathbf{_{MePS2}C_{MePS2}}$GUCAU<br>UGA AA 5′ | 73.2 ± 0.2 |

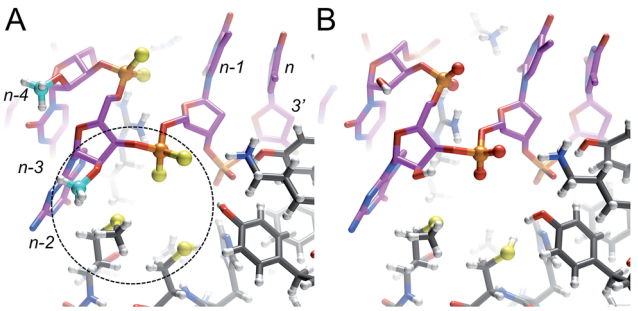


Fig. 4 Models of the interactions between the human Ago2 PAZ domain and the (A) MePS2-modified and (B) native siRNA sense strands. Only the 3′-terminal five residues of the RNA are shown (n-4 to n) and the TT-overhang is visible on the upper right in both panels. The formation of a hydrophobic patch between the Met-273 and Cys-270 side chains, methoxy moiety of $G_{n-2}$ and PS2 of $T_{n-1}$ is highlighted with a dashed circle in panel A. PS2 groups, sulfur atoms (yellow) and 2′-*O*-methyl carbons (cyan) are depicted in ball-and-stick mode and hydrogen atoms are white spheres of smaller radius. Note the significantly more polar environment of the phosphate (His, 2× Tyr, Lys) between overhanging dTs, visible on the right-hand side of the two panels.

To gain insight into the conformational consequences of PS2 modification and potential changes as a result of combining it with the ribose 2′-*O*-methyl substitution, we determined crystal structures of the RNA duplexes $(CGC_{PS2}GAAUUAGCG)_2$ ($C_{PS2}$G-RNA), $(CGCGA_{MePS2}AUUAGCG)_2$ ($A_{MePS2}$A-RNA), and $(CGCGAAUUA_{MePS2}GCG)_2$ ($A_{MePS2}$G-RNA) at resolutions of 1.19, 1.18 and 1.13 Å, respectively.‡ The structures were phased by molecular replacement, using the previously determined structure of the native RNA[16] as search model [ESI (Table S1†)].

The structures of the PS2-modified RNA duplexes are isomorphous with that of the native RNA.[16] Thus, the duplex is located on a crystallographic dyad and a single dodecamer strand constitutes the asymmetric unit. Residues are numbered 1–12 and those in the symmetry-related strand are numbered $1^{\#}$–$12^{\#}$ (Fig. 2). Superimposition of the $C_{PS2}$G and native RNA duplexes demonstrates their virtually identical conformations (Fig. S2†). In particular PS2 modification does not trigger any changes in the ribose conformation and the backbone torsion angles. The most obvious deviation concerns the P–S bond lengths in the phosphorodithioate moiety (*ca.* 1.94 Å) compared to the P–O bonds in the native phosphate (*ca.* 1.60 Å) (Fig. S2†).

In the $A_{MePS2}$A- and $A_{MePS2}$G-RNA duplexes, 2′-*O*-methyl groups are directed into the minor groove, a result of the familiar ap orientation around the C2′–O2′ bond (Fig. 3).[17,18] Therefore, neither the PS2 modification alone nor the combination of the PS2 and 2′-*O*-methyl modifications appear to have a notable effect on the conformation of A-form RNA judging from the crystallographic results.

However, the 2′-*O*-methyl modification can offset the slight thermodynamic destabilization caused by the PS2 moiety compared with the native RNA duplex.[10] We determined the melting temperatures ($T_m$) of siRNAs containing two to six MePS2 modifications and found that they exhibit thermal

Table 2 Human Ago2 binding affinities of EphA2 siRNAs with various sense strand modifications adjacent to the 3′-overhang

| siRNA ID | Sequence | $K_D$ |
|---|---|---|
| AF163A | 5′-UGA CAU GCC GAU CUA CAU$_{MePS2}$ G$_{MePS2}$**dTdT**-3′ | 21.1 |
| | 3′-Biotin **dTdT** ACU GUA CGG CUA GAU GUA C-5′ | pM[a] |
| AF163B | 5′-UGA CAU GCC GAU CUA CAU G**dTdT**-3′ | 0.6 μM |
| | 3′-Biotin **dTdT** ACU GUA CGG CUA GAU GUA C-5′ | |
| AF163C | 5′-UGA CAU GCC GAU CUA CAU$_{MePS}$ G$_{MePS}$**dTdT**-3′ | 41.1 nM |
| | 3′-Biotin **dTdT** ACU GUA CGG CUA GAU GUA C-5′ | |
| AF163D | 5′-UGA CAU GCC GAU CUA CAU$_{PS2}$ G$_{PS2}$**dTdT**-3′ | 12.4 |
| | 3′-Biotin **dTdT** ACU GUA CGG CUA GAU GUA C-5′ | pM[a] |
| AF163F | 5′-UGA CAU GCC GAU CUA CAU$_{PS}$ G$_{PS}$**dTdT**-3′ | 14.5 nM |
| | 3′-Biotin **dTdT** ACU GUA CGG CUA GAU GUA C-5′ | |

[a] The PS2- and MePS2-siRNA affinities based on bio-layer interferometry are similar, although those from cellular Ago2 association or pull-down assays consistently show tighter binding by MePS2-modified RNAs.[15]

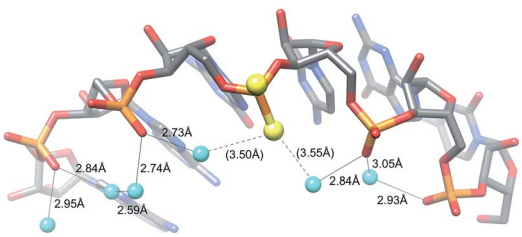


Fig. 5 The PS2 moiety disrupts H-bonding interactions in the water chain bridging adjacent O2P atoms in the major groove.

stabilities that are comparable to that of the unmodified RNA (PO2) (Table 1).

To assess potential conformational consequences of the MePS2 modification in solution, we measured the circular dichroism (CD) spectra of the siRNA duplexes listed in Table 1. All spectra were closely similar to the spectrum of the native duplex and are consistent with the typical A-type structure (a maximum of the positive Cotton effect at 268 nm and a cross-over point at 240 nm; Fig. S3†).

The lack of an obvious change in both the conformation and stability of MePS2-RNA relative to native RNA points to another cause of the favorable therapeutic properties of this modification.[15] To better understand the increased Ago2 affinity of siRNA containing MePS2-modified sense strands (Fig. S1†), we built models of PAZ–siRNA complexes† based on the crystal structure of a short RNA fragment featuring a 3′ two-residue overhang bound to the human Ago2 PAZ domain.[19] This domain is most likely the only region of Ago2 affected by MePS2 modification near the siRNA 3′-end (Fig. S4†). Comparison of the complexes with siRNA and MePS2-siRNA reveals formation of a hydrophobic patch in the latter, that involves both the 2′-*O*-methyl and PS2 moieties as well as methionine and cysteine side chains from the PAZ domain (Fig. 4). The hypothesis that increased hydrophobicity conferred by the MePS2 modification plays a key role in the stronger binding to Ago2 and its enhanced efficacy is supported by the relative Ago2 affinities of siRNAs containing no modification, PS, MePS, PS2 or MePS2 (Table 2).

## Conclusions

The MePS2 modification in the backbone region adjacent to the 3′-dTdT overhang of the siRNA sense strand triggers a strongly enhanced affinity to the RISC Ago2 slicer and silencing of proteins that confer chemoresistance in ovarian cancer cell lines and tumors.[15] This finding is surprising given the fact that the antisense siRNA strand mediates cleavage of the target RNA at the Ago2 active site and indicates that chemical modification of the sense strand can play a key role in siRNA loading and efficacy.

We demonstrate here that MePS2 modification does not affect RNA conformation and stability. Instead the increased Ago2 affinity is likely the result of favourable hydrophobic interactions with the PAZ domain mediated by both the 2′-*O*-methyl and PS2 moieties. This conclusion is consistent with the inability of PS2 sulphur atoms to form H-bonds with water molecules lining the RNA backbone in the crystal structure (Fig. 5).

Both steric and electronic factors can contribute to the increased nuclease resistance afforded by a modification.[18,20,21] The bulkier sulphur atoms in the PS2 moiety along with the increased hydrophobicity relative to PO2 might exclude non-thiophilic metal ions (*e.g.* $Mg^{2+}$) from an exonuclease active site or result in suboptimal positioning of the water nucleophile for attack at the phosphate group.

## Acknowledgements

Supported by US NIH grant R44 GM086937 (to X.Y. and M.E.).

## Notes and references

‡ Data deposition: final coordinates and structure factor files have been deposited in the Brookhaven Protein Data Bank (http://www.rcsb.org). The entry codes are 4RBY ($C_{PS2}$G-RNA), 4RBZ ($A_{MePS2}$A-RNA), and 4RC0 ($A_{MePS2}$G-RNA).

1 M. E. Davis, J. E. Zuckerman, C. H. J. Choi, D. Seligson, A. Tolcher, C. A. Alabi, Y. Yen, J. D. Heidel and A. Ribas, *Nature*, 2010, **464**, 1067–1070.
2 C. Pecot, G. Calin, R. Coleman, G. Lopez-Berestein and A. Sood, *Nat. Rev. Cancer*, 2011, **11**, 59–67.
3 J. C. Burnett, J. J. Rossi and K. Tiemann, *Biotechnol. J.*, 2011, **6**, 1130–1146.
4 J. Tabernero, G. I. Shapiro, P. M. LoRusso, A. Cervantes, G. K. Schwartz, G. J. Weiss, L. Paz-Ares, D. C. Cho, J. R. Infante, M. Alsina, M. M. Gounder, R. Falzone, J. Harrop, A. C. White, I. Toudjarska, D. Bumcrot, R. E. Meyers, G. Hinkle, N. Svrzikapa, R. M. Hutabarat, V. A. Clausen, J. Cehelsky, S. V. Nochur, C. Gamba-Vitalo, A. K. Vaishnaw, D. W. Sah, J. A. Gollob and H. A. Burris III, *Cancer Discovery*, 2013, **3**, 406–417.
5 S. Choung, Y. Kim, S. Kim, H. Park and Y. Choi, *Biochem. Biophys. Res. Commun.*, 2006, **342**, 919–927.

6 D. Bumcrot, M. Manoharan, V. Koteliansky and D. W. Y. Sah, *Nat. Chem. Biol.*, 2006, **2**, 711–719.
7 S. Shukla, C. S. Sumaria and P. I. Pradeepkumar, *ChemMedChem*, 2009, **5**, 328–349.
8 M. Manoharan, A. Akinc, R. K. Pandey, J. Qin, P. Hadwiger, M. John, K. Mills, K. Charisse, M. A. Maier, L. Nechev, E. M. Greene, P. S. Pallan, E. Rozners, K. G. Rajeev and M. Egli, *Angew. Chem., Int. Ed.*, 2011, **50**, 2284–2288.
9 D. M. Kenski, G. Butora, A. T. Willingham, A. J. Cooper, W. Fu, N. Qi, F. Soriano, I. W. Davies and W. M. Flanagan, *Mol. Ther.–Nucleic Acids*, 2012, **1**, e5.
10 X. Yang, M. Sierant, M. Janicka, L. Peczek, C. Martinez, T. Hassell, N. Li, X. Li, T. Wang and B. Nawrot, *ACS Chem. Biol.*, 2012, **7**, 1214–1220.
11 A. V. Lebedev and E. Wickstrom, *Perspect. Drug Discovery Des.*, 1996, **4**, 17–40.
12 W. S. Marshall and M. H. Caruthers, *Science*, 1993, **259**, 1564–1570.
13 A. Detzer, M. Overhoff, A. Mescalchin, M. Rompf and G. Sczakiel, *Curr. Pharm. Des.*, 2008, **14**, 3666–3673.
14 D. A. Braasch, Z. Paroo, A. Constantinescu, G. Ren, O. K. Öz, R. P. Mason and D. R. Corey, *Bioorg. Med. Chem. Lett.*, 2004, **14**, 1139–1143.
15 S. Y. Wu, X. Yang, K. Gharpure, H. Hatakeyama, M. Egli, M. McGuire, A. S. Nagaraja, T. Miyake, R. Rupaimoole, C. V. Pecot, M. Taylor, S. Pradeep, M. Sierant, C. Rodriguez-Aguayo, H. J. Choi, R. A. Previs, G. N. Armaiz-Pena, L. Huang, C. Martinez, T. Hassell, C. Ivan, V. Sehgal, R. Singhania, H.-D. Han, C. Su, J.-H. Kim, H. Dalton, C. Kowali, K. Keyomarsi, N. A. J. McMillan, W. W. Overwijk, J. Liu, J.-S. Lee, K. Baggerly, G. Lopez-Berestein, P. Ram, B. Nawrot and A. K. Sood, *Nat. Commun.*, 2014, **5**, 3459.
16 F. Li, P. S. Pallan, M. A. Maier, K. G. Rajeev, S. L. Mathieu, C. Kreutz, Y. Fan, J. Sanghvi, R. Micura, E. Rozners, M. Manoharan and M. Egli, *Nucleic Acids Res.*, 2007, **35**, 6424–6438.
17 P. Lubini, W. Zürcher and M. Egli, *Chem. Biol.*, 1994, **1**, 39–45.
18 M. Egli, G. Minasov, V. Tereshko, P. S. Pallan, M. Teplova, G. B. Inamati, E. A. Lesnik, S. R. Owens, B. S. Ross, T. P. Prakash and M. Manoharan, *Biochemistry*, 2005, **44**, 9045–9057.
19 J.-B. Ma, K. Ye and D. J. Patel, *Nature*, 2004, **429**, 318–322.
20 M. Teplova, S. T. Wallace, G. Minasov, V. Tereshko, A. Symons, P. D. Cook, M. Manoharan and M. Egli, *Proc. Natl. Acad. Sci. U. S. A.*, 1999, **96**, 14240–14245.
21 C. A. Brautigam, S. Sun, J. A. Piccirilli and T. A. Steitz, *Biochemistry*, 1999, **38**, 696–704.

# Supporting Information

# Crystal Structure, Stability and Ago2 Affinity of Phosphoro-dithioate-Modified RNAs

**Pradeep S. Pallan,[a] Xianbin Yang,*[,b] Malgorzata Sierant,[c] Nuwan Abeydeera,[b] Tom Hassell,[d] Carlos Martinez,[d] Barbara Nawrot,[c] and Martin Egli*[,a]**

[a]*Department of Biochemistry, Vanderbilt University School of Medicine, Nashville, TN 37232, USA.*

[b]*AM Biotechnologies LLC, 12521 Gulf Freeway, Houston, TX 77034, USA.*

[c]*Department of Bioorganic Chemistry, Centre of Molecular and Macromolecular Studies, Polish Academy of Sciences, Lodz, Poland.*

[d]*Sigma Life Science, 9186 Six Pines, The Woodlands, Texas 77380, USA.*

*E-mail: martin.egli@vanderbilt.edu; Fax: 1-615-322-7122; Tel: 1-615-343-8070, or E-mail: Xianbin.yang@thioaptamer.com Fax: 1-832-476-0294; Tel: 1-832-379-2175.

## Supporting Information Contents

**Synthesis of native and Me-, PS-, PS2- and MePS2-modified siRNAs**

The siRNA and modified RNAs were synthesized on an Expedite 8909 DNA/RNA Synthesizer using commercial 5′-DMT-2′-*O*-TBDMS nucleoside ($A^{Bz}$, $C^{Ac}$, $G^{Ac}$, and U) phosphoramidite monomers as well as 2′-*O*Me-thiophosphoramidites. The average stepwise coupling efficiency of all phosphoramidites including thiophosphoramidites was about 97% as estimated by the DMT-cation assay. After deprotection, all of the modified RNAs were isolated by FPLC according to a previously described protocol for purifying PS2-DNAs.[1,2] The PS2-RNAs were desalted using reverse-phase HPLC to yield the PS2-RNA final products. The representative structures of the MePS2-RNAs were confirmed by ESI-MS. Assembly of siRNA duplexes was performed in ammonium acetate buffer (pH 7.4) by heating the equivalent mixture of RNA oligonucleotides coding for the sense and antisense strands of siRNA at 90°C for 2 min, followed by slow cooling to room temperature (over 2 h). Assembly of the resulting duplexes was confirmed by electrophoresis using a 4% agarose gel.

**$T_m$ measurements**

All absorption measurements were performed in a 1-cm path length cell with a Cintra 4040 spectrophotometer equipped with a Peltier Thermocell (GBC, Dandenong, Australia). Complementary RNA strands were mixed in 10 mM Tris-HCl buffer (pH 7.4) with 100 mM NaCl, and 0.1 mM EDTA at a final concentration of 2 μM (0.8 OD of both mixed strands). The first step of the analysis was an annealing step from 85 to 15°C, with a temperature gradient of 1.5°C/min. Melting profiles were measured with a temperature gradient of 1°C/min, from 15 to 85 °C, with the detector set at 260 nm. Each $T_m$ reported was an average of values from three to six independent experiments.

**Ago2 affinity assays**

The antisense strand siRNA is biotinylated at its 3′-terminus, allowing immobilization of an annealed duplex on to a streptavidin (SA) coated sensor surface. This enables kinetic analysis of siRNA duplex binding to Ago2 on a fortéBIO Octet Red96 instrument set at 30°C. Samples were agitated at 1000 rpm. The annealing method, binding buffer condition, siRNA loading concentration, siRNA loading time, Ago2 titer range, appropriate blocking reagent, blocking time, Ago2 stability over assay duration, and octet baseline correction methods were thoroughly investigated and optimized in the current study. Ago2 in HSCMT was prepared as a dilution series (0, 12.5, 25, 50, 100, and 200 nM) along with HSCMT buffer blanks (unloaded sensor controls). Association was monitored for 300 sec and dissociation was followed for 300 sec. If necessary, the dissociation was stretched to at least 900 sec to verify tight

binding. The data were fit to a 1:1 binding model using fortéBIO Octet data analysis software. Kinetic constants were determined by integration of the experimental data using the differential rate equation $dR/dt = k_{on} \cdot C \cdot (R_{max}-R) - k_{off} \cdot R$ to obtain both the $k_a$ and $k_d$ values ($R$ = observed response, $R_{max}$ = maximum response upon saturation, $C$ = analyte concentration, $k_{on}$ = association rate constant, $k_{off}$ = dissociation rate constant). The ratio between $k_{off}$ and $k_{on}$ corresponds to the reported dissociation constants ($k_{off}/k_{on}=K_D$). The goodness of the fit was judged by the reduced $\chi^2$ and $R^2$ values.

**CD measurements**

CD spectra were recorded on a CD6 dichrograph (Jobin-Yvon, Longjumeau, France) using cells with 0.5 cm path length, 2 nm bandwidth, and 1-2 sec integration time. Each spectrum was smoothed with a 25-point algorithm (included in the manufacturer′s software, version 2.2.1) after averaging of at least three scans. The spectra from 200 nm to 340 nm were recorded at 25°C in the same buffer used for the melting experiments. The concentration of the two complementary RNA oligonucleotides was ca. 2 μM.

**Modeling of PAZ:siRNA complexes**

Coordinates for the crystal structure of a self-complementary RNA with a 3′-dCT overhang bound to the human Ago2 PAZ domain[3] were obtained from the Protein Data Bank (http://www.rcsb.org/pdb/home/home.do; PDB ID 1si2). Using the program UCSF Chimera[4] non-canonical Py:Py and Pu:Pu pairs were replaced by Watson-Crick pairs according to the EphA2 siRNA sequence (**Fig. S1**, **Table 2**), and the 2′-deoxy-C in the 3′-overhang was replaced by T. In addition all water molecules were removed and hydrogen atoms were added. Following rebuilding of the RNA, the native complex was subjected to minimization by steepest descent and conjugate gradient using the Amber ff12SB force field in Chimera. In the complex with the MePS2-modified sense strand, two phosphates adjacent to the 3′-overhang were replaced by phosphorodithioate moieties (taken from the crystal structure of $C_{PS2}$G-RNA). In addition, methyl groups were added to the 2′-oxygen atoms, such that the conformation of the $CH_3$-O2′-C2′-C3′ torsion angle is in the *antiperiplanar* range. The complex was subsequently subjected to refinement as described above for the native PAZ:siRNA complex.

**Crystallization experiments**

The modified RNA dodecamers r(CGC$_{PS2}$GAAUUCGCG) [$C_{PS2}$G-RNA], r(CGCGA$_{MePS2}$AUUAGCG) [$A_{MePS2}$A-RNA] and r(CGCGAAUUA$_{MePS2}$GCG) [$A_{MePS2}$G-RNA] were dissolved in deionized water and the stock concentrations adjusted to ca. 1.2 mM. Crystallization trials were performed with the

hanging drop vapor diffusion technique, using the 24 conditions of the Nucleic Acid Miniscreen (Hampton Research Inc., Aliso Viejo, CA).[5] Droplets (1 μL) of modified RNA dodecamer were mixed with droplets of equal volume of the individual sparse matrix screen solutions and equilibrated against 0.6 mL of a 35% v/v solution of 2-methyl-2,4-pentanediol (MPD) at 18°C. The optimal crystallization conditions for the three oligonucleotides were as follows. $C_{PS2}$G-RNA: condition 20; sodium cacodylate buffer, pH 7.0, 80 mM sodium chloride, 20 mM barium chloride, 12 mM spermine tetrahydrochloride, and 10% v/v MPD. $A_{MePS2}$A-RNA: condition 15; 40 mM sodium cacodylate pH 7.0, 12 mM spermine tetrahydrochloride, 80 mM potassium chloride, and 10% v/v MPD. $A_{MePS2}$G-RNA: condition 8; 40 mM sodium cacodylate, pH 6.0, 80 mM sodium chloride, 12 mM spermine tetrahydrochloride, and 10% v/v MPD.

**X-ray data collection, structure determination and refinement**

Crystals were mounted in nylon loops, flash-frozen in liquid nitrogen without further cryo-protection and stored in liquid nitrogen prior to data collection. Diffraction data were collected on the 21-ID-F or 21-ID-G beam lines of the Life Sciences Collaborative Access Team (LS-CAT) at the Advanced Photon Source (APS), located at Argonne National Laboratory (Argonne, IL), using MARCCD 225/300 detectors. The wavelength was 0.98 Å and crystals were kept at 100K during data collection. Diffraction data were integrated, scaled and merged using HKL2000.[6] Selected data collection and refinement statistics are listed in **Table S1**. The structure was determined by the molecular replacement method with the program MOLREP[7] in the CCP4 suite of crystallographic software,[8] using the native RNA dodecamer as the search model (PDB ID 2Q1R[9]; http://www.rcsb.org). Following initial positional and isotropic temperature factor refinements with the program REFMAC,[10] the R-work dropped to the mid 20s and R-free to the upper 20s. After further refinement in REFMAC, refinements were continued with SHELX.[11] The phosphorodithioate and 2'-*O*-methyl moieties (the asymmetric unit contains a single strand) were built into Fourier ($2F_o$-$F_c$) sum and ($F_o$-$F_c$) difference electron density maps that were visualized with COOT[12] and the refinement was continued after adaptation of the dictionary files. Further refinements were carried out and after each refinement the nucleotides and water molecules were checked for possible alternate conformations/positions and corrections were made where necessary. A final refinement was carried out with all nucleic acid atoms and water molecules being treated with anisotropic B-factors and these refinement parameters are summarized in **Table S1**. All figures were generated with the program UCSF Chimera.[4]

**Table 1.** Selected crystal data and refinement parameters for PS2- and MePS2-modified RNAs

| **Structure** | $C_{PS2}$G-RNA | $A_{MePS2}$A-RNA | $A_{MePS2}$G-RNA |
|---|---|---|---|
| **Crystal data** | | | |
| Space group | | Monoclinic *C*2 | |
| Unit cell constants | | | |
| *a* [Å] | 40.93 | 41.18 | 40.91 |
| *b* [Å] | 35.02 | 35.05 | 34.84 |
| *c* [Å] | 31.87 | 31.85 | 32.27 |
| $\beta$ [deg] | 128.8 | 128.7 | 127.5 |
| No. of strands per asym. unit | 1 | 1 | 1 |
| No. of unique reflections | 11,133 | 11,706 | 12,267 |
| Resolution [Å] (last shell) | 1.19 (1.23-1.19) | 1.18 (1.22-1.18) | 1.13 (1.17-1.13) |
| Completeness [%] (last shell) | 97.7 (88.5) | 99.9 (100) | 95.5 (90.7) |
| R-merge [%] (last shell) | 5.0 (4.2) | 8.2 (21.6) | 5.3 (25.5) |
| **Refinement** | | | |
| R-work / R-free | 0.139 /0.183 | 0.160/0.201 | 0.181/0.208 |
| No. of RNA atoms | 256 | 258 | 258 |
| No. of water molecules | 97 | 70 | 52 |
| No. of metal ions | 2 $Sr^{2+}$ [a] | - | - |
| R.m.s. deviations: | | | |
| Bond lengths [Å] | 0.012 | 0.011 | 0.012 |
| Bond angles [Å] [b] | 0.03 | 0.036 | 0.040 |
| **Data deposition** | | | |
| PDB ID | 4RBY | 4RBZ | 4RC0 |

[a] Refinement suggested $Sr^{2+}$ ions with occupancy 0.3. This is in contrast to the crystallization conditions.
[b] 1…3 distance based on SHELX refinement.

Sense 5'-UGACAUGCCGAUCUACAU$_{MePS2}$G$_{MePS2}$TT-3'
Antisense 3'-TTACUGUACGGCUAGAUGUA C-5'

**Fig. S1.** Sequence of the EphA2 siRNA with two sense-strand MePS2 modifications.

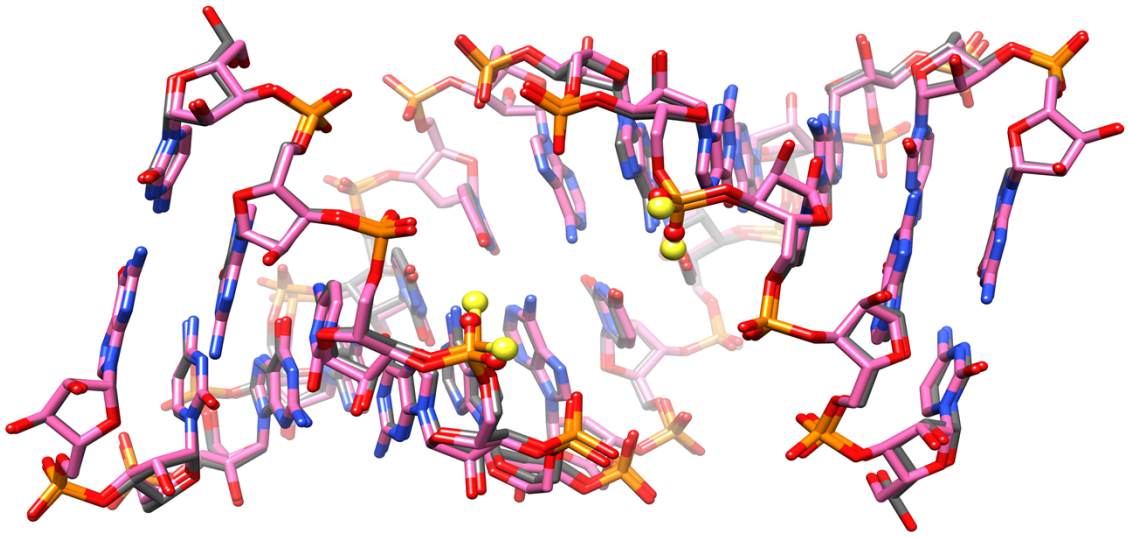

**Fig. S2.** Superimposition of the native (pink carbon atoms; PDB ID 2q1r) and $C_{PS2}G$ RNA dodecamer crystal structures (gray carbon atoms).

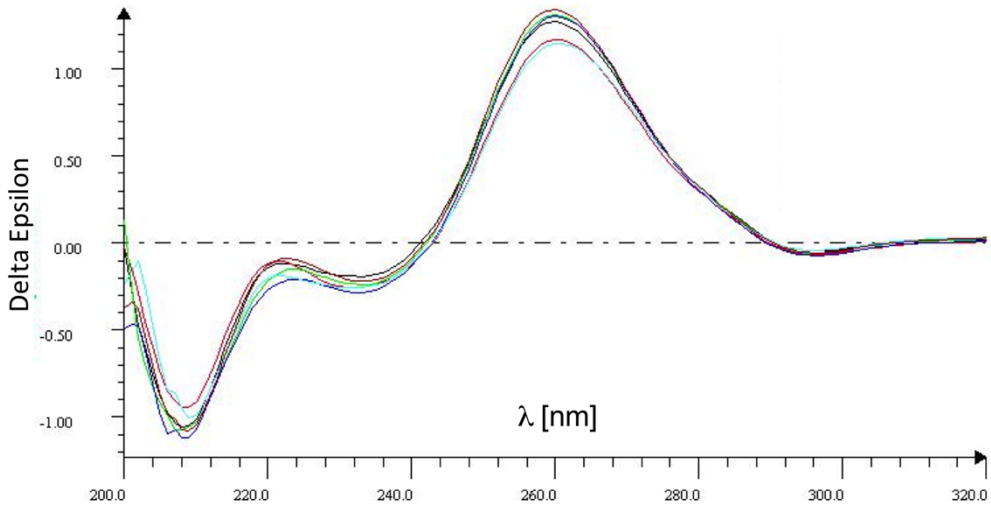


**Fig. S3.** CD spectra of the native RNA duplex siRNA-1 (for sequences see **Table 1**; purple), and MePS2-modified RNA duplexes MePS2-1 (black), MePS2-3 (red), MePS2-4 (green), MePS2-9 (blue), and MePS2-11 (cyan).

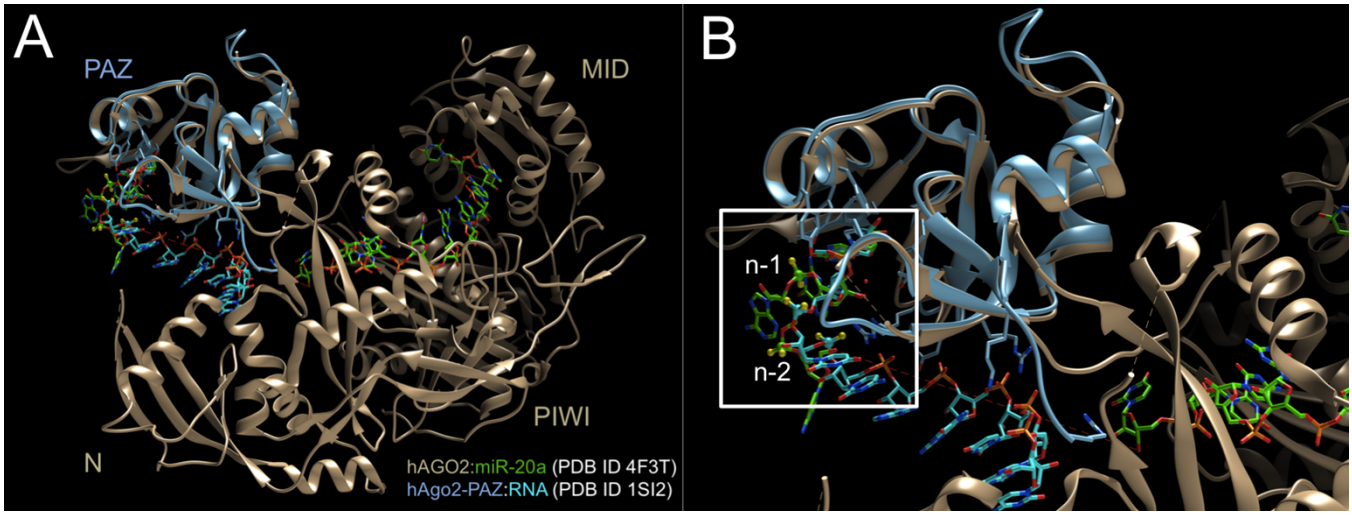


**Fig. S4.** (A) Overall and (B) close-up views of superimposed crystal structures of the complexes between the human AGO2 PAZ domain and a self-complementary 9mer (cyan) with a 3′-dCT overhang[3] (PDB ID 1si2), and between human AGO2 and miR-20a RNA (green)[13] (PDB ID 4f3t). The images illustrate that the interactions between the 3′-end of siRNAs and the PAZ domain can be analyzed in an isolated fashion. The region of the structure analyzed in the context of the MePS2 modifications at the n-1 and n-2 phosphates and shown in **Fig. 4** in the main paper is boxed in panel B and phosphates are labeled. The mid-section of the green RNA strand (dotted red line) is not visible in electron density maps of the Ago2:miR-20a complex.

**References**


1. Yang, X.; Sierant, M.; Janicka, M.; Peczek, L.; Martinez, C.; Hassell, T.; Li, N.; Li, X.; Wang. T.; Nawrot, B. *ACS Chem. Biol*. **2012**, *7*, 1214-1220.
2. Wu, S. Y.; Yang, X.; Gharpure, K.; Hatakeyama, H.; Egli, M.; McGuire, M.; Nagaraja, A. S.; Miyake, T.; Rupaimoole, R.; Pecot, C. V.; Taylor, M.; Pradeep, S.; Sierant, M.; Rodriguez-Aguayo, C.; Choi, H. J.; Previs, R. A.; Armaiz-Pena, G. N.; Huang, L.; Martinez, C.; Hassell, T.; Ivan, C.; Sehgal, V.; Singhania, R.; Han, H.-D.; Su, C.; Kim, J.-H.; Dalton, H.; Kowali, C.; Keyomarsi, K.; McMillan, N. A. J.; Overwijk, W. W.; Liu, J.; Lee, J.-S.; Baggerly, K.; Lopez-Berestein, G.; Ram, P.; Nawrot, B.; Sood, A. K. *Nat. Comm.* **2014**, *5*, 3459.
3. Ma, J.-B.; Ye, K.; Patel, D. J. *Nature*, **2004**, *429*, 318-322.
4. Pettersen, E. F.; Goddard, T. D.; Huang, C. C.; Couch, G. S.; Greenblatt, D. M.; Meng, E. C.; Ferrin, T. E. *J. Comp. Chem.* **2004**, *25*, 1605-1612.
5. Berger, I.; Kang, C. H.; Sinha, N.; Wolters, M.; Rich, A. *Acta Cryst. D* **1996**, *52*, 465-468.
6. Otwinowski, Z.; Minor, W. *Meth. Enzymol.* **1997**, *276*, 307-326.
7. Vagin, A.; Teplyakov, A. *J. Appl. Crystallogr.* **1997**, *30*, 1022-1025.
8. Collaborative Computational Project, Number 4. The CCP4 suite: programs for protein crystallography. *Acta Cryst. D*, **1994**, *50*, 760-763.
9. Li, F.; Pallan, P. S.; Maier, M. A.; Rajeev, K. G.; Mathieu, S. L.; Kreutz, C.; Fan, Y.; Sanghvi, J.; Micura, R.; Rozners, E.; Manoharan, M.; Egli, M. *Nucleic Acids Res.* **2007**, *35,* 6424-6438.
10. Murshudov, G. N.; Vagin, A. A.; Dodson, E. J. *Acta Cryst. D* **1997**, *53*, 240-255.
11. Sheldrick, G. M. Methods Enzymol. **1997,** 276, 628-641.
12. Emsley, P.; Cowtan, K. *Acta Cryst. D* **2004**, *60*, 2126-2132.
13. Elkayam, E.; Kuhn, C. D.; Tocilj, A.; Haase, A. D.; Greene, E. M.; Hannon, G. J.; Joshua-Tor, L. *Cell* **2012**, *150*, 100-110.


**Acknowledgements**


The project upon which this publication is based was performed pursuant to an agreement with AM Biotechnologies, LLC which in turn was supported by a Grant Number 2R44 GM086937-03 from the National Institutes of Health. Use of the Advanced Photon Source (APS) was supported by the U. S. Dept. of Energy, Office of Science, Office of Basic Energy Sciences, Contract No. DE-AC02-06CH11357.